Coastal Engineering 58 (2011) 837–850

Contents lists available at ScienceDirect

Coastal Engineering

journal homepage: www.elsevier.com/locate/coastaleng

Breaking solitary wave evolution over a porous underwater step

Javier L. Lara *, Inigo J. Losada, Maria Maza, Raul Guanche

Environmental Hydraulics Institute "IH Cantabria", Universidad de Cantabria, Avda. de los Castros s/n. 39005 Santander, Spain

ARTICLE INFO

Article history:
Received 11 February 2011
Received in revised form 19 April 2011
Accepted 2 May 2011
Available online 21 June 2011

Keywords:
Solitary wave evolution
Tsunami wave
Solitary wave fission
Porous media flow
Navier–Stokes models
Wave breaking

ABSTRACT

Solitary wave evolution over a shelf including porous damping is investigated using Volume-Averaged Reynolds Averaged Navier–Stokes equations. Porous media induced damping is determined based on empirical formulations for relevant parameters, and numerical results are compared with experimental information available in the literature. The aim of this work is to investigate the effect of wave damping on soliton disintegration and evolution along the step for both breaking and non-breaking solitary waves. The influence of several parameters such as geometrical configuration (step height and still water level), porous media properties (porosity and nominal diameter) or solitary wave characteristics (wave height) is analyzed. Numerical simulations show the porous bed induced wave damping is able to modify wave evolution along the step. Step height is observed as a relevant parameter to influence wave evolution. Depth ratio upstream and downstream of the edge appears to be the more relevant parameter in the transmission and reflection coefficients than porosity or the ratio of wave height–water depth. Porous step also modifies the fission and the solitary wave disintegration process although the number of solitons is observed to be the same in both porous and impermeable steps. In the absence of breaking, porous bed triggers a faster fission of the incident wave into a second and a third soliton, and the leading and the second soliton reduces their amplitude while propagating. This decrement is observed to increase with porosity. Moreover, the second soliton is released before on an impermeable step. Breaking process is observed to dominate over the wave dissipation at the porous bottom. Fission is first produced on a porous bed revealing a clear influence of the bottom characteristics on the soliton generation. The amplitude of the second and third solitons is very similar in both impermeable and porous steps but they evolved differently due to the effect of bed damping.

© 2011 Elsevier B.V. All rights reserved.

1. Introduction

Propagation and transformation of a solitary wave over a submerged obstacle have been deeply studied in literature. Works have been motivated due to the fact that solitary wave transformation on a shelf is a critical problem when evaluating effects produced by tsunami waves in coastal areas. Related processes such as wave run-up or wave induced forces on coastal structures are conditioned by nonlinear wave transformation while propagating onshore due to bottom bathymetry geometry and seabed physical properties. According to the analysis of wave transformation by bathymetry, most of the studies have been focused on an abrupt change on the seabed. Wave transformation over a step has been commonly adopted as a reference scenario. Losada et al. (1989) classified the solitary wave evolution on an impermeable shelf by distinguishing four types of wave behavior: (1) propagation with weak distortion, (2) fission of the wave in solitons, (3) fission in solitons and peaking (breaking) of the first soliton and (4) plunging of the wave and evolution of the subsequent bore with development of and undulation on the rear side of the broken wave.

Solitary wave propagation without distortion is not of great interest from wave evolution point of view. Most of the analytical studies, Whitham (1974) or Mei (1985), have focused on the second and third modes studying scattering of solitary waves and their later evolution. More recently, Pelinovsky et al. (2009) studied the fission processes generated on a submerged step with both Korteweg–de Vries (KdV) and Boussinesq equations. A Navier–Stokes (NS) type equation with a k-ε model was also used in order to show the degree of accuracy of the different approaches. Solitary wave celerity was predicted differently by Boussinesq and Navier–Stokes equations observing some lag between them.

Solitary wave evolution under breaking conditions has traditionally been studied by means of experimental analysis due to the complexity of the breaking processes. Seabra-Santos et al. (1987) and Losada et al. (1989) detected that if breaking appears after the beginning of the fission process, fission is still active. Losada et al. (1989) also identified an oscillation on the rear side of the broken wave. They also presented a diagram combining theoretical and experimental work to define the four evolution modes as a function of the normalized incident wave height and step geometry.

Liu and Cheng (2001) used an NS-type model with a k-ε turbulence closure scheme, to study numerically solitary wave fission. They observed differences in the generation of second and third solitons under wave breaking conditions.

* Corresponding author. Tel.: +34 942 20 18 10; fax: +34 942 20 18 60.
E-mail address: lopezjav@unican.es (J.L. Lara).

0378-3839/$ – see front matter © 2011 Elsevier B.V. All rights reserved.
doi:10.1016/j.coastaleng.2011.05.008

In the previously presented analysis, bottom physical properties, such as roughness or permeability were not taken into account. It is well known that porous seabed generates wave damping and nonlinear processes while propagating over rough or porous seabeds. Putnam (1949) was one of the first to determine the loss of energy due to percolation on a permeable sea bottom assuming Darcy's law. Two of the most used experimental works on wave damping were conducted by Savage (1953) and Sawaragi and Deguchi (1992). Both experiments were done using periodic wave conditions. Attenuation by bed friction and percolation, boundary layer behavior and nonlinear effects on incident waves were investigated. Recently, a new set of experiments on monochromatic waves has been carried out by Corvaro et al. (2010) on smooth, rough and porous seabeds. Influence of the geometric properties of the porous bed (thickness and length) on wave height attenuation was also reported. Using a numerical approach, a modified version of the KdV equation was derived by Mei and Li (2004) to characterize long wave propagating over a randomly rough bottom. New terms representing the effects of disorder on amplitude attenuation and wave phase were introduced to model solitons fission phenomena.

The use of Navier–Stokes-type equations has become popular in the last decade to address wave transformation studies, not only because they solve the complete velocity field but also because they overcome most of the simplifications behind wave theories. The highly non-linear and highly dispersive nature of the Navier–Stokes equations allows modeling complex wave transformation processes. Moreover, they do not require empirical formulations in order to trigger breaking and to determine the breakpoint location such as it is required for Boussinesq-type models. In terms of solitary wave damping, Huang et al. (2008) analyzed the numerical accuracy of a two-dimensional N-S model when simulating solitary wave propagation over porous beds. Turbulence and wave breaking were not considered in the simulations. Wave damping was found to increase with porosity close to 0.5. Larger or lower porosity induced less energy loss on the wave field. Both Huang et al. (2003) and Lin (2004) presented a numerical study of solitary wave interaction with submerged rectangular permeable structures based on NS equations. Flow percolation was considered in both cases, however only Lin (2004) considered turbulent processes into the equations. Solitary wave evolution, energy reflection, transmission and dissipation were investigated. However, soliton disintegration was not observed in the simulations due to the finite dimension of the submerged step.

In this paper, a numerical investigation of the evolution of a solitary wave on a permeable submerged step is considered. The main objective is to investigate the effect of wave damping on soliton disintegration and evolution processes over the step for both breaking and non-breaking solitary waves. For nonbreaking waves and impermeable bottom numerical results will be compared with experimental information available in the literature for model validation. Reflection, transmission, energy damping and soliton fission will be described according to the porous material characteristics. Due to the complexity of the wave breaking and the flow percolation processes, an NS model will be used. IH-2VOF model presented by Lara et al. (2010) is able to solve simultaneously the flow in the porous media and in the clear region (outside the porous media) by means of the Volume-Averaged Reynolds Averaged Navier–Stokes equations (VARANS).

2. Numerical model description

IH-2VOF (Lara et al., 2010) is the tool employed in this paper to investigate the solitary wave propagation over porous steps. IH-2VOF solves wave flow for hybrid domains in a coupled NS-type equation system, at the clear-fluid region (outside the porous media) and inside the porous media. The movement of free surface is tracked by the Volume of fluid (VOF) method.

At the clear-fluid region 2DV Reynolds Average Navier–Stokes (RANS) equations are considered. Turbulence is modeled using a k-ε equation model for the turbulent kinetic energy (k), and the turbulent dissipation rate (ε). The influence of turbulence fluctuations on the mean flow field is represented by the Reynolds stresses. The governing equations for k-ε are derived from the Navier–Stokes equations, and higher order correlations of turbulence fluctuations in k and ε equations are replaced by closure conditions. A nonlinear algebraic Reynolds stress model is used to relate the Reynolds stress tensor and the strain rate of mean flow. Volume of fluid (VOF) method is followed to track free surface.

The flow inside the porous media is modeled by the resolution of the Volume-Averaged Reynolds Averaged Navier–Stokes (VARANS) equations first presented by Hsu et al. (2002). These equations are derived by integrating the RANS equations over a control volume, and their final form is presented below:

$$\frac{\partial \overline{u_i}}{\partial x_i} = 0 \tag{1}$$

$$\frac{1+c_A}{n}\frac{\partial \overline{u_i}}{\partial t} + \frac{\overline{u_j}}{n^2}\frac{\partial \overline{u_i}}{\partial x_j} = -\frac{1}{\rho}\frac{\partial \overline{p_0}}{\partial x_i} + \frac{\nu}{n}\frac{\partial^2 \overline{u_i}}{\partial x_j \partial x_j} - \frac{1}{n^2}\frac{\partial \overline{u_i' u_j'}}{\partial x_j} - \frac{\alpha\nu(1-n)^2}{n^3 D_{50}^2}\overline{u_i} - \frac{\beta(1-n)}{n^3 D_{50}}\overline{u_i}\,\overrightarrow{|u|}\,. \tag{2}$$

In the previous equations, variables t, u and p_0 denote time, Reynolds averaged velocity and effective pressure ($p_0 = p + \rho g_i x_i$, where p is pressure and g is gravitational acceleration) respectively, n is the porosity, ρ is the density, ν is the kinematic viscosity, i and j represent the horizontal and vertical directions, the over-bar represents volume averaged, single and double primes are Reynolds averaged fluctuation and volume averaged fluctuation respectively. Volume averaged velocity is called seepage velocity. As can be seen, clear fluid porosity becomes unity and VARANS equations yield into the traditional RANS equations. In the VARANS equations, a k-ε model is adopted to consider turbulent effects. The k- ε model is selected among the different turbulence models existing in the literature because it is the only one available with a porous flow closure adopted from Nakayama and Kuwahara (1999) and previously validated by several authors as Hsu et al. (2002), Lara et al. (2006a), Lara et al. (2006b) or Losada et al. (2008) among others.

The two last terms on the right hand side of Eq. (2) model the interfacial drag forces created by the solid skeleton of the porous media. They are known as the extended Forchheimer relationship. The first linear term represents a Darcy's flow type behavior. The second term models the non-linear characteristics of the flow when it becomes turbulent. They are expressed in terms of the porosity, nominal diameter (D_{50}), kinematic viscosity (ν) and two empirical coefficients α and β. In the VARANS equations an inertia force is also introduced in terms of the added mass coefficient affecting the first term on the left hand side of Eq. (2), where $c_A = \gamma_p \frac{1-n}{n}$ is the added mass coefficient and γ_p is adopted to be 0.34 (van Gent, 1995). This term accomplishes the additional momentum damping when the flow is accelerated within the porous media.

Coefficients α and β have to be written in terms of the porous material properties based on empirical approximations because of the lack of a formulation or theory which relates the physical properties of the stone material and the flow characteristics. Although some attempts have been done in order to describe the physical process of porous induced drag (see Burcharth and Andersen, 1995), the high number of parameters involved in the physics and also the random nature of some of them, such as stone shape and sorting material, make the problem very difficult to be solved. However, in order to consider the variation α and β coefficients with the porous material characteristics, a formulation is presented in this work based on

empirical formulations. Simplified equations are used in order to get a formulation able to predict α and β coefficients within the range of suggested values in literature.

According to Sollitt and Cross (1972), a Forchheimer relationship can be written in terms of the permeability coefficient (K_p), a porous drag coefficient (C_f) and the seepage velocity as follows:

$$F_{porous\_drag} = \frac{\nu}{K_p}\overline{u_i} + \frac{C_f}{\sqrt{K_p}}\overline{u_i}\,|\overrightarrow{\overline{u}}|. \tag{4}$$

According to McDougal (1993), permeability coefficient (K_p) can be related with nominal diameter and porosity:

$$K_p\left(m^2\right) = 1.643\cdot 10^7\left(\frac{D_{50}(mm)}{10}\right)^{1.57}\frac{n^3}{(1-n)^2}. \tag{5}$$

Moreover, the non-linear drag force coefficient C_f is evaluated following Arbhabhirama and Dinoy (1973):

$$C_f = 100\left(D_{50}(m)\sqrt{\frac{n}{K_p}}\right)^{1.5}. \tag{6}$$

Using a correspondence between the extended Forchheimer relationship and Eqs. (5) and (6), coefficients α and β can be written in terms of the nominal diameter (in m) and porosity as:

$$\alpha = 4409.22\cdot D_{50}^{0.43} \text{ and } \beta = 12.27\cdot\frac{n^3}{(1-n)^{1.5}}D_{50}^{-0.1075}. \tag{7}$$

Eq. (7) is used in this work to describe the flow damping characteristics according to the granular bed physical properties, nominal diameter and porosity. Parameters obtained with Eq. 7 are within the range of values proposed by Burcharth and Andersen (1995).

IH2-VOF uses a finite difference scheme to discretize the equations. A forward time difference and a combined central difference and upwind schemes are considered for the time and spatial derivations respectively. A two-step projection method is used in the resolution of the equations. The turbulence model is solved based on an explicit finite difference scheme.

Wave conditions are introduced in the model imposing a velocity field and a free surface time evolution on one side of the numerical domain. Active wave absorption can also be considered, not only at the rear end of the numerical flume to allow waves leave the domain but also at the wave generating boundary so as not to interfere with the generated waves. In this work, solitary waves are generated following the Boussinesq formulation proposed by Lee et al. (1982). The formulation is based on analytical solutions of the velocity field and free surface that are used as an input to the model.

As will be explained, the numerical model used in this study and earlier versions has gone through a series of rigorous quantitative verifications and validations.

3. Numerical model validation

Although the current model and its previous versions have been extensively validated for several wave dynamics such as wave breaking on gravel beaches (Lara et al., 2006b); hydrodynamics of natural (Torres-Freyermuth et al., 2007) and artificial barrier beaches (Torres-Freyermuth et al., 2010) and wave and permeable coastal structures interaction (i.e.: Lara et al., 2006a; Losada et al., 2008; Guanche et al., 2009), further validation is required for the specific problem tackled in this work. As a consequence, two numerical experiments have been carried out using physical model experiments available in the literature.

As a preliminary step, solitary wave evolution over a submerged impermeable step is simulated and compared with experimental data provided by Seabra-Santos et al. (1987) similarly as reported by Liu and Cheng (2001). Next, in an attempt to assess the accuracy of the model simulating wave damping on permeable seabeds, experimental results reported in Sawaragi and Deguchi (1992) are compared with numerical results.

In this work, Seabra-Santos et al. (1987) experiments were simulated considering the full 36 m long flume. The 0.10 m high step was placed 18 m from the wave paddle. After a sensitivity analysis of the cell size and corresponding aspect ratio, a uniform 1 cm (H) × 0.5 cm (V) grid size was used.

Comparisons between numerical and experimental ratios of the incident (A_i) and transmitted (A_t) amplitudes against water depth in front of the step (d_0) of the first and second solitons are given in Fig. 1. Different d_0 conditions in front of the step have been considered. Shallow water results presented by Seabra-Santos et al. (1987) are also included in the different panels. Twenty seven different cases, grouped in five different water depth conditions are plotted. As can be seen, the numerical model gives predictions that are in very good agreement with the experimental data from corresponding tests. The model is able to predict with high accuracy the leading and second soliton generation for different water depth conditions. Both experimental data and numerical results presented here show lower values than shallow water solutions.

Comparisons of the time history of free surface profiles are displayed in Fig. 2 for a case with $d_0 = 20$ cm and $A_i = 3.65$ cm. Panels show results at four positions along the step, x = 0 (step location), 3, 6 and 9 m, respectively. Free surface is normalized by water depth in front of the step (d_0). Overall agreement is reasonable although some variations can be observed. These small deviations can be attributed to the differences between the numerical and physical wave generation procedures and are apparent in panel 1 corresponding to x = 0 (junction location). In general, the volume of water transported by the solitary wave seems to be lower in the numerical model. While fission appears and solitons propagate, larger discrepancies are observed. Indeed, although soliton amplitude is predicted with high accuracy, a phase lag is observed. Results show the same pattern observed by Seabra-Santos et al. (1987) and Liu and Cheng (2001): the leading soliton seems to propagate faster than in the numerical solution. However, in this work, variations in the second soliton celerity are more significant. As reported in Liu and Cheng (2001) experiments might contain slight errors. It may be reasonable to suppose that the difference in the shape of the incident wave profile pointed out before and small variations in the location of the gauges in the experiments may be the source of the observed discrepancies.

As a further validation, solitary wave propagation over a permeable bed is then considered on comparisons with experimental data reported by Sawaragi and Deguchi (1992). Although only monochromatic waves were considered in the experiments, the validation is carried out using these experiments because of the lack of experimental tests of wave damping in solitary waves on permeable bottoms. In the experiments wave attenuation is produced by a 3.5 m long and 15 cm thick permeable layer made of 3.07 cm nominal diameter permeable material. Since the porosity was not provided in the paper $n = 0.4$ has been used, based on the estimation reported by Chang (2004) for the same experiments. Two cases, with H = 3.6 cm and T = 1.0 s and H = 3.6 cm and T = 1.5 s, are numerically simulated. A uniform 1 cm (H) × 0.5 cm (V) grid size is used after a sensitivity analysis. The porous flow parameters have been calculated using Eq. (7), yielding $\alpha = 985.89$ and $\beta = 2.45$, which are in the order of magnitude proposed by Burcharth and Andersen (1995).

Comparisons between numerical (solid line) and experimental (dotted line) results are shown in Fig. 3. The ratio between local wave height and incident wave height is plotted in the middle and lower panels, for $H = 3.07$ cm and $T = 1.0$ s and $H = 3.07$ cm and $T = 1.5$ s,

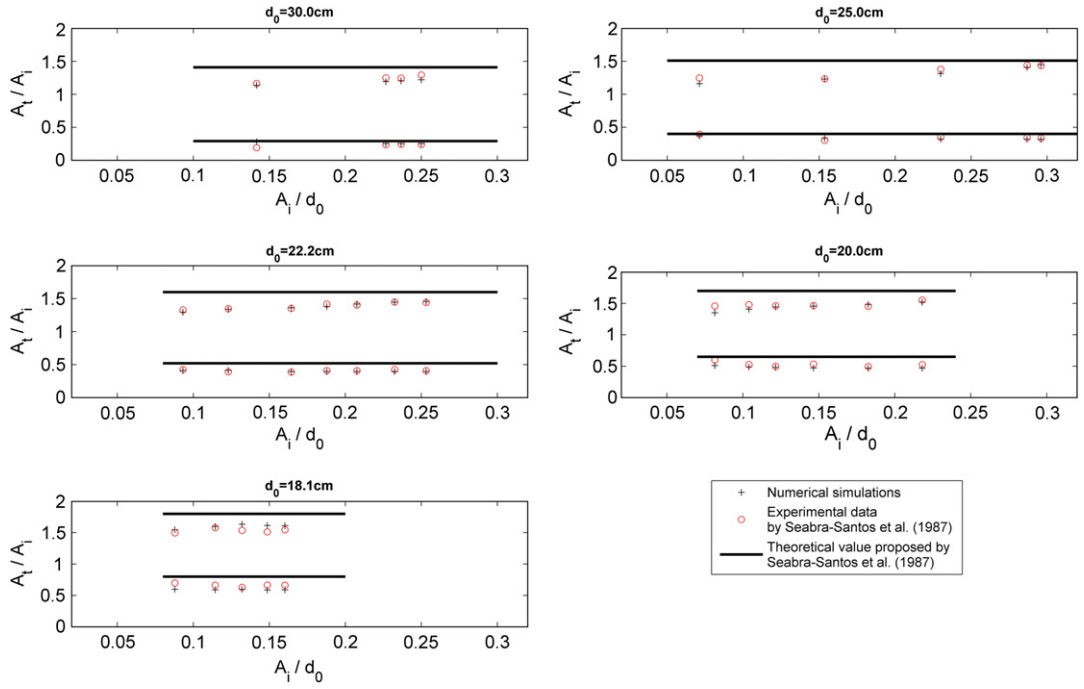

Fig. 1. Comparison between experimental data from Seabra-Santos et al. (1987) and numerical simulations of amplitude of ratios of the incident (A_i) and transmitted (A_t) amplitudes of first and second solitons for different still water level conditions (d_0).

respectively. As evident in Fig. 3, numerical results are in good agreement with laboratory data for both cases considered. Wave attenuation is estimated to be reduced approximately 40% at the end of the porous bed. Since no detailed measurements of the free surface were reported for the damping process, wave profile comparisons cannot be presented here. However, numerical solutions of the free surface evolution along the flume are plotted in the upper panel. In order to achieve a better view of the wave attenuation pattern, the free surface has been multiplied by a factor of two. Wave damping is clearly evident while waves are propagating over the porous bed. Two important features can be identified from the simulations. First, a regular wave crest–trough pattern is lost while the wave is propagating over the porous bed as a consequence of the non-linear wave–bed interaction processes. Second, an increase of mean water level is observed at the region downstream the porous bed, as a result of the bed-induced friction.

The results presented in this section together with previous tests reported in the literature demonstrate the feasibility of numerically addressing the study of breaking and nonbreaking solitary waves on a porous underwater step using IH2-VOF.

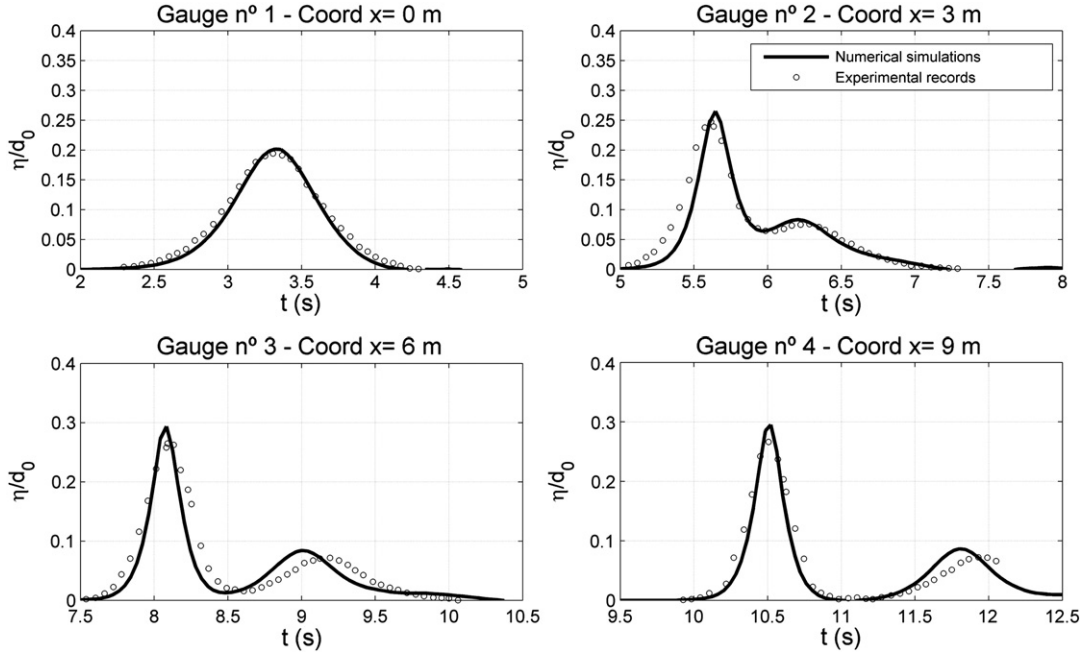

Fig. 2. Comparisons of time history of free surface for experimental data from Seabra-Santos et al. (1987) and numerical simulations for $d_0 = 20$ cm and $A_i = 3.65$ cm.

4. Numerical experiments of breaking and nonbreaking solitary waves

4.1. Numerical setup

A set of numerical experiments has been carried out to analyze the evolution of a solitary wave on a permeable submerged step. The aim is to investigate the effect of wave damping on soliton disintegration and evolution over the step for both breaking and non-breaking solitary waves. A 36 m long and 0.6 m high numerical wave flume has been the standard for simulations. Fig. 4 shows a schematic diagram of the numerical setup. After a sensitivity analysis, a uniform grid system of $\Delta x = 0.01$ m and $\Delta y = 0.005$ m is used. A step with a variable depth (d), located 4 m away from the inflow boundary, has been employed in order to produce the four evolution modes described by Losada et al. (1989): (1) propagation with weak distortion, (2) fission of the wave in solitons, (3) fission in solitons and peaking (breaking) of the first soliton and (4) plunging of the wave and evolution of the subsequent bore with development of and undulation on the rear side of the broken wave. While the water depth ($h_1 = 0.3$ m) in front of the step has been kept constant for all the numerical experiments, the water depth over the step (h_2) varied according to the step height. Six step heights are considered with the following depth ratios, $h_1/h_2 = 1.2$, 1.5, 2, 3, 4 and 5. Incident solitary wave heights (H) are defined as follows: $H/h_2 = 0.1$, 0.2, 0.3, 0.4, 0.5 and 0.6. Active wave absorption is considered at the generation boundary and at the rear end of the wave flume, so as not to affect the solitary wave evolution within the numerical flume. Both impermeable and permeable steps are used. Impermeable steps are used as reference cases to obtain a better understanding of wave evolution on permeable steps. Porous media characteristics are set to include four porosity conditions ($n = 0.3$, 0.4 0.5 and 0.6) and three nominal diameter ($D_{50}/h_1 = 0.05$, 0.1 and 0.2). Corresponding values of linear and non-linear drag parameters were defined according to Eq. (7).

As a consequence a total of 468 numerical experiments are performed on a standard PC. The computational cost is 1 h per simulation. The length of each of the simulations is set at 35 s in order to allow waves to reach the rear end of the computational domain.

4.2. Analysis of solitary wave evolution along the step

Solitary wave evolution along the step is discussed first. A schematic diagram of the numerical domain and the definition of the most important variables are presented in Fig. 4. Figs. 5, 6 and 7 show several snapshots of solitary wave free surface for impermeable (solid line) and porous steps (dashed line). The free surface is normalized by the target wave height. In the horizontal axis relative distances to water depth in front of the step are plotted. The larger nominal diameter ($D_{50}/h_1 = 0.2$) and porosity n = 0.5 are chosen because porous damping effects are anticipated to be more visible. Results for small ($h_1/h_2 = 1.2$ and 1.5), medium ($h_1/h_2 = 2$ and 3) and high ($h_1/h_2 = 4$ and 5) steps are presented in Figs. 5, 6 and 7, respectively. This allows classifying results according to the expected solitary wave transformation and to the number of generated solitions on an impermeable step with the same geometry. Following Whitham (1974), two solitons are expected for $h_1/h_2 = 1.2$ and 1.5, three for $h_1/h_2 = 2$, 5 for $h_1/h_2 = 3$, four for $h_1/h_2 = 4$ and seven for $h_1/h_2 = 5$.

Fig. 5 provides the first evidence of the differences between wave transformation on impermeable and permeable steps. The solitary wave does not break in any of the simulated cases on the small steps except for the case presented in panel (f). A weak spilling breaker is observed for the higher wave height $H/h_1 = 0.5$. For the impermeable step, wave symmetry is practically preserved for the leading soliton, especially for cases $H/h_1 = 0.3$ and 0.5 (panels b and c). Wave peaking

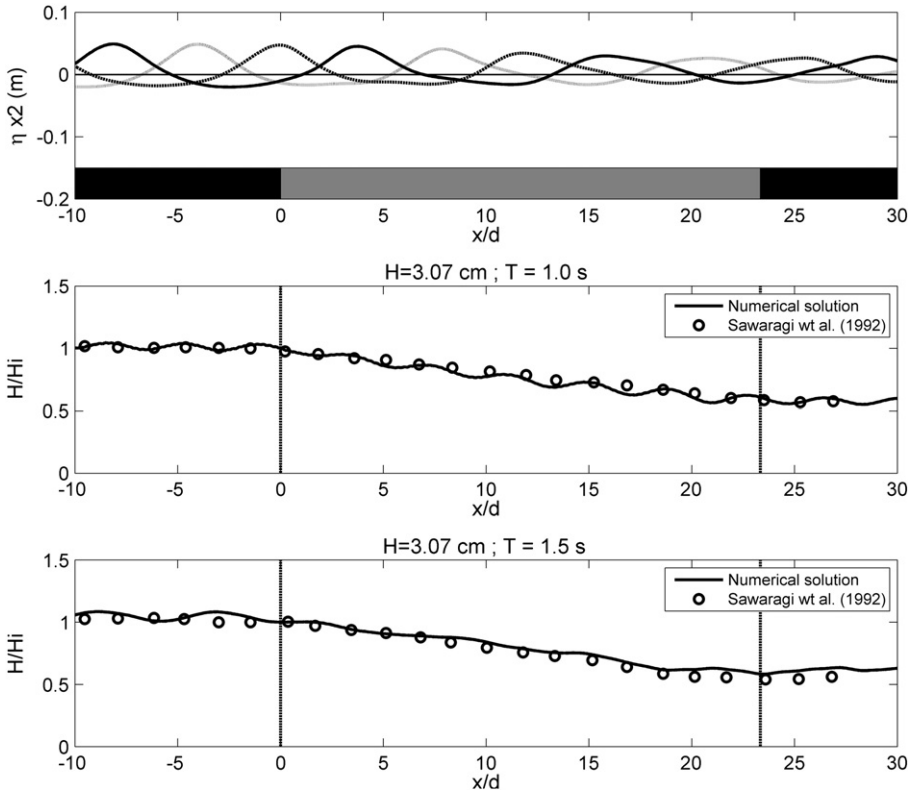

Fig. 3. Comparisons of wave damping on monochromatic waves between numerical data and Sawaragi and Deguchi (1992) experiments. Upper panel: numerical solutions of free surface evolution along the flume. Middle panel: H = 3.07 cm and T = 1.0 s. Lower panel: H = 3.07 cm and T = 1.5 s.

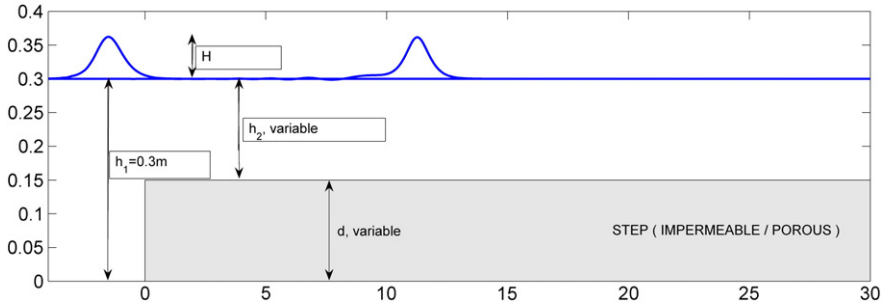

Fig. 4. Setup of the numerical experiments.

is more significant for $h_1/h_2 = 1.5$ (panels d, e and f) reaching values close to $\eta_{max}/H = 1.26$ in contrast to $\eta_{max}/H = 1.1$ for the smallest step (panels a, b and c). Fission takes place according to the expected solution and two solitons can be identified. This is more evident in the three lower panels. Wave damping is present in all the simulations shown in the figure. Additionally, damping effects appear to be more important for the smaller wave height increasing with step height. Another important feature can be observed in panels a and c, namely that waves propagate faster over a porous step than over an impermeable step if wave non-linearity is small, as confirmed in panel a. However, when wave non-linearity increases, wave celerity decreases when compared with impermeable steps. This effect can be explained using the effective water depth concept, h_{ef}, first introduced by Losada et al. (1997). In their work, the effective water depth over a porous step was a fundamental parameter to define the influence of structure permeability on potential harmonic generation. It was shown that for a given incident wave and structure geometry the chance of harmonic generation is reduced with increasing porosity. A similar interpretation can be made to explain the differences observed in solitary wave celerity and fission triggering for impermeable and porous steps.

In the first case (panel a), wave-induced velocities within the porous step are smaller and wave damping is also smaller. The effective water depth in this situation is larger than the one over the impermeable step, since due to the step permeability the wave founds a higher water column and the wave propagates faster. However, when non-linearity increases, wave-induced flow within the porous step produces larger damping yielding wave height reduction and consequent lower wave celerity. The effective water depth in this last case is closer to that of the impermeable step case.

Results for the medium step heights are presented in Fig. 6. Panels a, b and c correspond to $h_1/h_2 = 2$. Peaking is observed to increase compared to results already presented in Fig. 5. According to Losada et al. (1989) fission into three solitons is expected. Moreover, they predicted that the larger waves will shoal and break as a spilling breaker. Panel (a) indicates that numerical results are consistent with the said prediction, since wave heights increase to values close to $\eta_{max}/H = 1.5$ and fission is developed generating three solitons. In addition, panels b and c show that the model also predicts a spilling breaker.

Relevant differences can be observed between impermeable and porous steps. In the first case, presented in panel a, wave height reduction due to the bed friction is almost 80% according to the impermeable bed solution. Although fission takes place over a porous bed, the leading soliton shows a smaller amplitude than the second soliton at locations larger than $x/h_1 > 80$. Moreover, even if a coherent fission is still visible, solitons do not show a peaked and narrow wave profile as that of the impermeable step. Another interesting feature can be extracted from panel b. Although wave breaks over the impermeable step, breaking is not observed on the permeable step. Bed-induced damping decreases wave height and breaking does not develop. Wave reduction by the porous bed is also observed to be more significant than the one observed for the solitary wave over the impermeable step. For panel c, the solitary wave breaks over both impermeable and porous steps.

Wave evolution plotted in panels d, e and f, in Fig. 6 and in every panel of Fig. 7 shows a similar behavior. Since step height increases, the solitary wave breaks even closer to the beginning of the step. Wave breaking changes from spilling to plunging and the number of solitons grows when decreasing the depth over the step. For the larger wave height and the higher steps, wave breaks sooner and fission does not take place (see panel f, Fig. 7), generating a broken bore as the one observed by Losada et al. (1989). If the wave is not as high, wave fission can be developed later over the step (see panels b, c and d, Fig. 7). Wave behavior over the porous step is affected more significantly by damping and most of the wave energy is dissipated over the step. Although, fission takes place, the solitons amplitude is very small. They do not develop or grow as they do on an impermeable bed. The damping mechanism created by the porous bed can even make the solitons disappear while propagating on the step.

The role of porosity is further investigated in Fig. 8. Wave evolution over two porous steps ($n = 0.5$, dashed line; $n = 0.3$, solid line) and identical nominal diameter ($D_{50}/h_1 = 0.2$) is analyzed. Results for three wave characteristics corresponding to $H/h_1 = 0.1$ (panel a), 0.3 (panel b) and 0.5 (panel c) are plotted in the figure. As expected, the influence of porosity in wave propagation is evident in the three panels. Porous bed damping increases with porosity, even in the presence of breaking, as observed in panel c. In the neighborhood of the step small differences are found in wave amplitude and shape, even for the broken waves (panel c). These differences are due to the flow percolated inside the porous step. For $n = 0.5$, larger wave-induced flow is observed within the porous step. Wave fission takes place independently of bed porosity. Variations of soliton generation with porosity have not been found. However, soliton celerity appears to be clearly affected by bottom induced damping, because of the direct relation between wave height and solitary wave celerity. Nominal diameter influence on wave propagation and fission (not shown here) exhibits the same characteristics as those observed for varying porosity. Wave damping increases with the nominal diameter while wave height and soliton celerity decreases.

The relative importance of the breaking process and the porous bed in terms of momentum damping is presented next. A spilling broken solitary wave is investigated in order to better visualize turbulence levels in the physical process. Plunging breakers are generated when water depth over the step is lower and a clear difference of both turbulence sources, breaking and porous step, cannot be identified. Fig. 9 presents a solitary wave breaking evolution over $n = 0.5$ porous step for $h_1/h_2 = 3$ and $H/h_1 = 0.5$. Black patches represent turbulent kinetic energy (k) normalized by solitary wave celerity over the water depth in front of the step. As can be seen in the figure higher turbulence values are found at the broken wave front than in the porous step. Although turbulence is clearly generated within the porous bed, their importance is lower in momentum

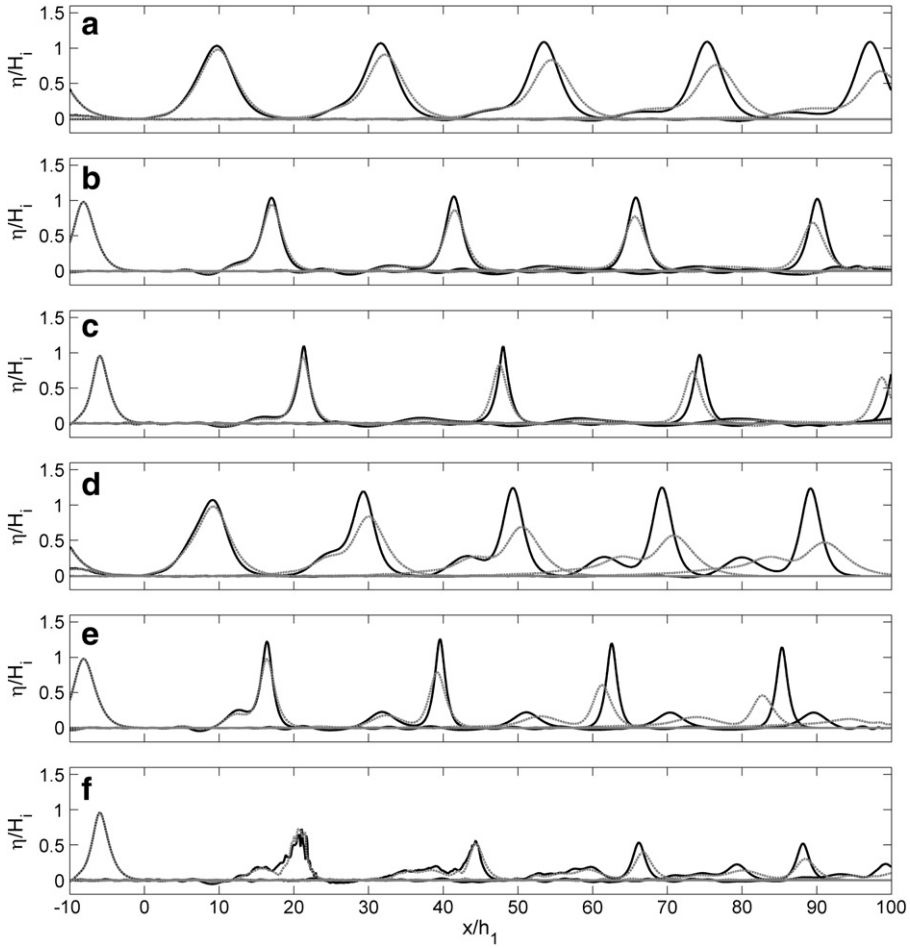

Fig. 5. Solitary wave evolution along the numerical flume for impermeable (black solid line) and porous (n = 0.5, $D_{50}/h_1 = 0.2$, dashed line) small steps. $h_1/h_2 = 1.2$ (panels a, b and c), 1.5 (panels d, e and f). $H/h_1 = 0.1$ (panels a and d), 0.3 (panels b and e) and 0.5 (panels c and f).

damping than in the breaking process are reported by Lara et al. (2006a) for regular wave breaking on gravel slopes. Momentum damping mechanism within the porous media is driven by porous drag terms. Larger turbulence levels can be identified close to the porous step upper edge due to the velocity gradient generated at the clear fluid–porous bed interface.

4.3. Wave reflection and transmission

The effect of step porosity on wave reflection and transmission is researched next. Solitary wave evolution depends highly on wave transformation in the vicinity of the step. In the near field, reflection dominates upstream the step. Downstream, the wave is affected by energy losses localized at the step due to flow separation. Far from the front edge of the step, the wave is split into solitons and non-linear and dispersive effects dominate wave propagation. As discussed previously, porous bed induced damping is also very relevant to understand wave evolution. The range of variation of the leading wave and the secondary solitons is highly affected by damping. Moreover, wave dynamics differs significantly from a porous to an impermeable step, as part of the wave penetrates through the porous media. Porosity and non-linear damping influence flow discharge.

In this work, the analysis of wave transmission and reflection is focused at the step edge. Definitions introduced by Goring (1979) are followed. As anticipated by Goring (1979) and later confirmed by many experimental works such as Losada et al. (1989) and numerical studies, such as Huang et al. (2003), solitary wave increases in front of the step reaching a maximum amplitude. As the wave is propagating on the step, the wave decreases first because flow accelerates due to water depth reduction, increasing again when the leading wave accommodates to the new depth. Although wave breaking may also occur, it never appears at the step front edge.

In this study, the transmission coefficient is expressed in terms of the ratio of the free surface decrement just after the step (H_{min}) and the incident wave height (H_i) as H_{min}/H_i. The reflection coefficient is measured close to the generation boundary, and is given as the ratio between the reflected and incident wave heights, H_r/H_i.

Numerical results of transmission are presented in Fig. 10 for $D_{50}/h_1 = 0.2$ and different incident wave conditions. For comparison impermeable and porous steps results are plotted together. In this analysis, h_2/h_1 was used instead of h_1/h_2, as in previous sections, in order to better visualize the results.

In general, transmission is shown to increase as the step height decreases as expected. These results are consistent with Seabra-Santos et al. (1987) work over impermeable steps. Indeed, the H_{min}/H_i ratio is observed to be very close in all the simulated cases to those cases in which the step height h_2/h_1 was larger than 0.4. Several transmitted wave ratios are obtained depending on the non-linearity of the wave. Values of H_{min}/H_i between 0.85 and 0.95 are reached. However, differences were more visible for the three higher steps. The transmitted wave height decreases due to the energy loss at the step. Moreover, the role of the porous step is more significant and the transmitted wave appears to be larger than over impermeable steps. This feature can be explained because part of the wave induced flow penetrates through the porous step and yielding a lower transmission coefficient. The transmission coefficient in a porous step is observed to

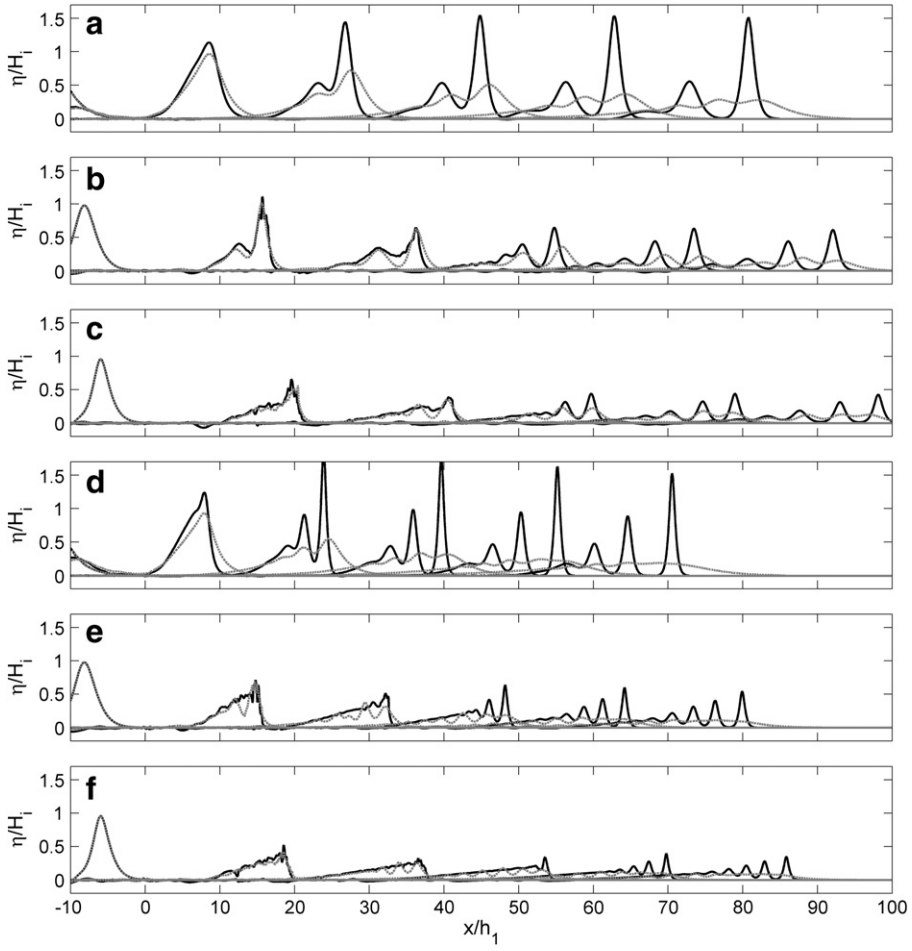

Fig. 6. Solitary wave evolution along the numerical flume for impermeable (black solid line) and porous (n = 0.5, $D_{50}/h_1 = 0.2$, dashed line) medium steps. $h_1/h_2 = 2$ (panels a, b and c), 3 (panels d, e and f). $H/h_1 = 0.1$ (panels a and d), 0.3 (panels b and e) and 0.5 (panels c and f).

be about 5% larger than in the impermeable step. Slight differences are observed with varying porosity. It is also of interest to note that numerical simulations show a different behavior for the smaller wave height cases (upper left panel). For these cases, the transmission coefficient appears to be larger over the impermeable step. This feature can be explained with the formation of a partially standing wave due to the reflection at the step. Wave height increases due to reflection in a higher rate in the impermeable step than in the four porous steps due to the action of percolation and dissipation. Moreover, results from Fig. 11 clearly show that the depth ratio h_2/h_1 is a more relevant parameter in the transmission coefficient than porosity or relative wave height H_i/h_1. Indeed, the transmission coefficient varies slightly for h_2/h_1 larger than 0.4 and for H_i/h_1 larger than 0.5.

Numerical reflection coefficients are plotted in Fig. 11 for porous ($D_{50}/h_1 = 0.2$) and impermeable steps. Panels are organized according to step geometry to visualize changes with relative incident wave height (H_i/h_1). Generally speaking, the reflection coefficient decreases with increasing H_i/h_1. Slight variations are observed for the lower step height geometries ($h_1/h_2 = 1.5$). However, larger reflection coefficient variations are observed for the higher steps ($h_1/h_2 = 5$), due to viscous damping effects. The formation of a aforementioned partially standing wave can be easily identified by the larger values of reflection coefficient for the higher steps. The presence of a porous step induces a lower reflection coefficient, which varies with step and wave height. An explanation of this behavior can be found considering the effect of the percolating flow through the step. Indeed, higher differences in reflection coefficients between impermeable and porous steps are found for higher steps in which flow percolation is more important.

4.4. Leading soliton evolution

After having analyzed the wave behavior in the neighborhood of the step, wave evolution downstream of the edge of the step is investigated in this section. The main focus is set on studying the leading solution evolution over different porous steps. The impermeable step case is used as a reference to better understand the role of wave damping effects induced by the porous materials. Figs. 12 and 13 show the leading soliton evolution for one impermeable and two porous steps (n = 0.3 and 0.5, $D_{50}/h_1 = 0.2$) over six different geometries. For each of the figures nine different panels are plotted including different geometries and incident wave conditions. Panels in the same column represent wave evolution over the same geometry. Wave height to water depth ratio (H_1/h) is kept constant for panels in the same row with varying step geometry. Three different wave conditions are plotted here, $H_i/h_1 = 0.1$, 0.3 and 0.5.

The leading soliton evolution along the step for the lower wave height can be seen in panels a, d and g both in Figs. 12 and 13. A weak distortion in wave height is evident for the two lower impermeable steps (panels a and d, Fig. 12). Wave height is slightly increased by the presence of the step. Moreover, wave peaking is observed for higher steps. Indeed, wave breaking occurs as the step height is increased (panels d and g, Fig. 13) with a consequent sudden wave height reduction. As expected the porous step induces wave damping. As in previous analysis, damping is predicted to increase with porosity for a given geometry.

As can be seen in Fig. 12, wave evolution for $H_i/h_1 = 0.3$ is predicted to be similar to the smaller wave height ratio. However, an

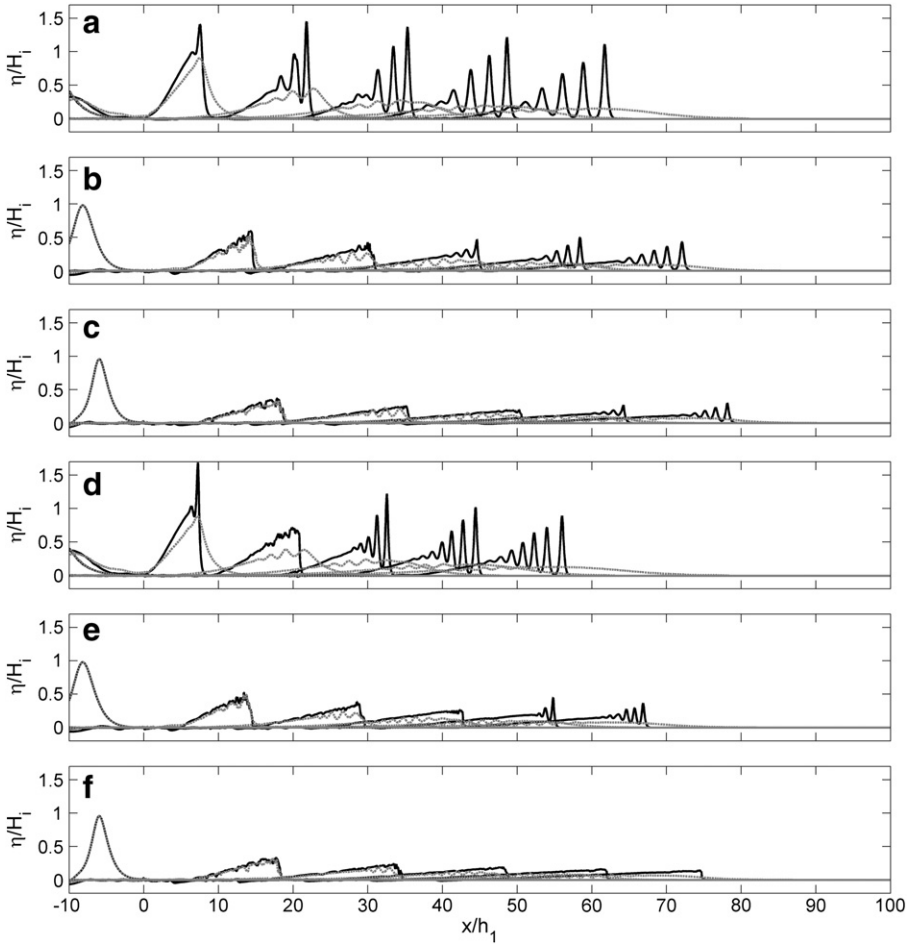

Fig. 7. Solitary wave evolution along the numerical flume for impermeable (black solid line) and porous (n = 0.5, $D_{50}/h_1 = 0.2$, dashed line) high steps. $h_1/h_2 = 4$ (panels a, b and c), 5 (panels d, e and f). $H/h_1 = 0.1$ (panels a and d), 0.3 (panels b and e) and 0.5 (panels c and f).

increasing non-linearity results in new processes. Under these conditions, wave breaking takes place for a lower impermeable step than in the previous case as can be seen in panel h, Fig. 12. However, under the same conditions, wave breaking is not developed along both porous steps. Increasing step heights (panels b, e and h in Fig. 13) results in breaking for both impermeable and porous steps. Minor differences in the location and magnitude of the maximum wave height are visible. Energy dissipation at porous steps induces a different behavior for wave evolution over impermeable and porous steps, even during the breaking process. Waves over impermeable steps show a more visible curly shape due to the existence of an oscillating broken bore also detected experimentally by Losada (1997) and confirmed numerically by Liu and Cheng (2001). After breaking, the wave damping role is also visible. A smoother wave

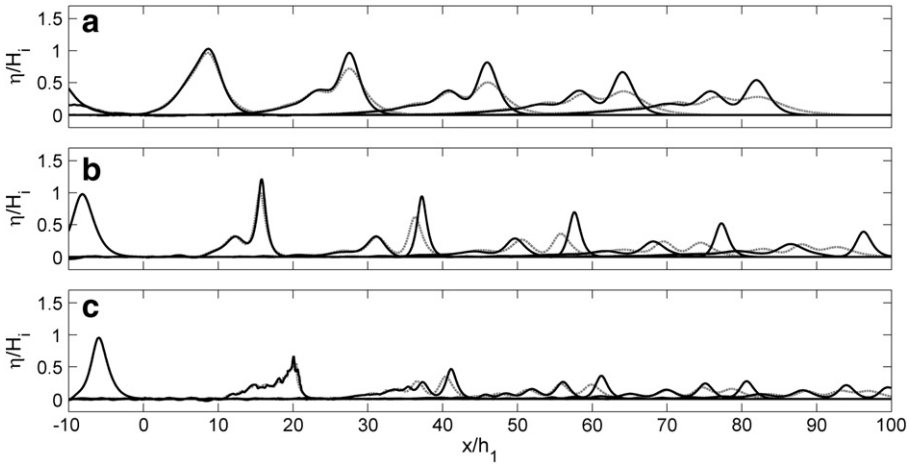

Fig. 8. Solitary wave evolution along the numerical flume for porous step (n = 0.5, $D_{50}/h_1 = 0.2$, dashed line; n = 0.3, $D_{50}/h_1 = 0.2$, solid line); $h_1/h_2 = 2$ (panels a, b and c); $H/h_1 = 0.1$ (panel a), 0.3 (panel b) and 0.5 (panel c).

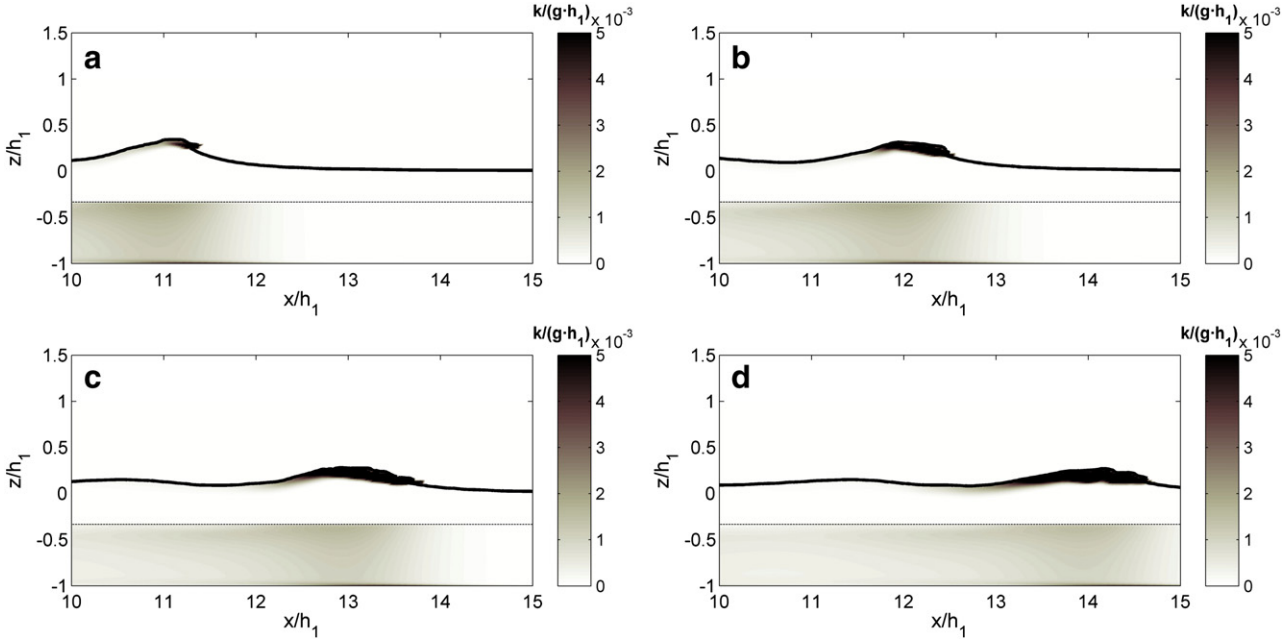

Fig. 9. Normalized turbulent kinetic energy (k) for a solitary broken wave ($H/h_1 = 0.3$ and $D_{50}/h_1 = 0.3$) over a porous step ($n = 0.5$).

profile is obtained for the porous bottom case due to the induced damping, noted in panels (panels b, e and h in Fig. 13). Although an oscillating bore is created, energy dissipation at the bed arises as an important feature in terms of energy sink. Wave evolution after breaking also appears to be influenced by damping, and wave height decreases with increasing porosity. Most of the energy is dissipated in the higher step as shown in panel h (Fig. 13).

Larger wave height cases (panels a, f, and i in Fig. 13) confirmed the description already presented. However, due to the larger energy of the wave at the breaking point compared with previous cases, differences in the breaking point location (location of the maximum wave height) and the evolution post-breaking of the leading solitons are smaller between porous and impermeable steps. Behavior appears to be very close to either impermeable or porous cases. Slight differences in the shape of the evolution of the wave along the step, including breaking and post-breaking, are found. This can be attributed to a weaker influence of the bed induced damping compared with the energy carried by the wave.

4.5. Solitons evolution

In order to complete the analysis, fission and solitons evolution is presented next. Six cases are chosen according to the solitary wave evolution pattern. Figs. 14 and 15 contain the evolution of the amplitudes of the leading, second and third solitons at the upper, medium and lower panels respectively. Three solitary wave amplitudes are chosen, corresponding to $H_i/h_1 = 0.1$, 0.3 and 0.5. Results for a $h_1/h_2 = 2$ step are plotted in Fig. 13 and for a $h_1/h_2 = 3$ step in Fig. 15. According to Whitham (1974), 3 solitons are expected for $h_1/h_2 = 2$ and 5 for $h_1/h_2 = 3$. Solitons evolution over an impermeable step is plotted with a solid line. Dashed and dotted lines are used for $n = 0.5$ and $D_{50}/h_1 = 0.2$ and $n = 0.5$ and $D_{50}/h_1 = 0.2$ respectively.

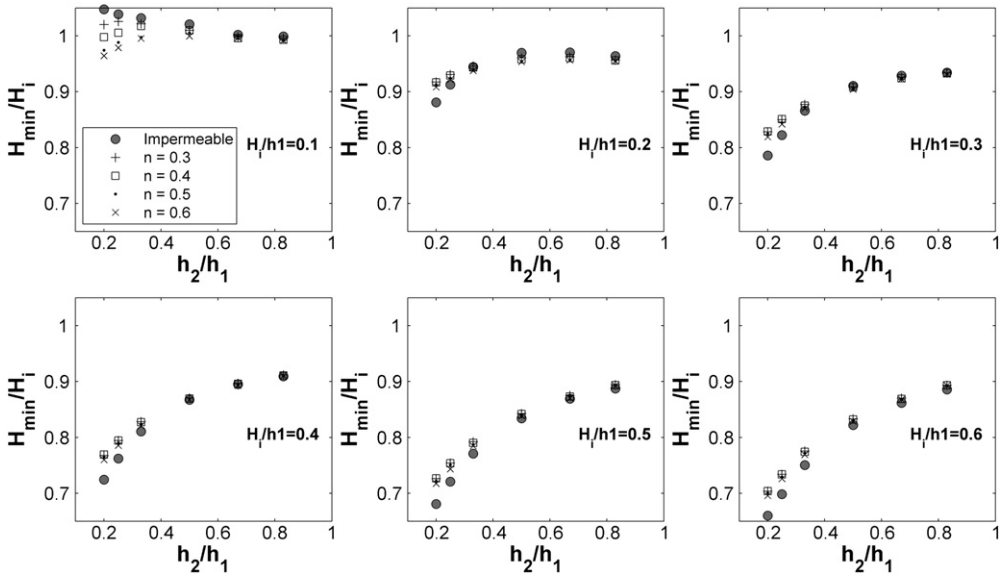

Fig. 10. Normalized solitary wave elevation in the neighborhood of the step for $D_{50}/h_1 = 0.2$. Several step characteristics (impermeable and porous) are plotted together.

Fig. 14 contains three cases in which the effect of the porous bed on the solitons evolution along the step is clearly visible. Three different situations are represented: non-breaking waves (first column panels), breaking only on the impermeable step (middle column panels) and breaking (right column panels). As expected, three solitons can be seen in all the cases.

For the smaller incident solitary wave (panels in the left column), a strong dissipation is observed for the leading soliton amplitude along the porous steps. Although the main soliton increases its amplitude along the impermeable step, the second and the third achieved a constant height, as it was stated by Liu and Cheng (2001). Solitons evolution along the porous step diverges for the second soliton (middle panel) due to the action of the porous bed. The amplitude decreases along the step and damping is observed to increase with porosity. Wave dissipation on the third soliton is not significant due its smaller amplitude, showing a constant value. An important characteristic is also observed: the second soliton is first released on an impermeable step. It can be also seen at the left column panel in Fig. 15.

Wave breaking takes place along the step for increasing solitary wave amplitude as can be seen in the middle column panels for $H_i/h_1 = 0.3$, only for the impermeable step. As reported by Liu and Cheng (2001), the fission process occurs before breaking. The second soliton seems to evolve independently from the broken bore which travels faster. Once the bore height is reduced significantly, the newly formed leading wave propagates downstream with constant amplitude. The growth of the second soliton and the decreasing amplitude of the third one, while propagating downstream, imply transference of energy between them.

When breaking occurs on both impermeable and porous steps, wave fission and further evolution is more or less similar, with a rapid decrease of the leading wave amplitude and the generation of the second and third solitions. However, fission is produced first on a porous bed revealing a clear influence of the bottom characteristics on the soliton generation. The amplitude of the second and third solitons is very similar in all the cases however they evolved differently due to the effect of bed damping. In this case, wave breaking appears closer to the step edge and the second soliton is not released before breaking. Although some dissipation and flow percolation within the porous media is affecting wave transformation, incident wave height and step height appear to be the most important parameters to determine fission and breaking characteristics on the step. Results presented in Fig. 15 also confirm this point. Due to a larger relative step height h_1/h_2, the breaking process is even closer on the middle and right column cases. Fission is also observed closer to the step edge on porous bottoms. This effect is amplified with porosity.

5. Conclusions

Previous work has documented the process of solitary wave transformation including soliton fission both experimentally and numerically.

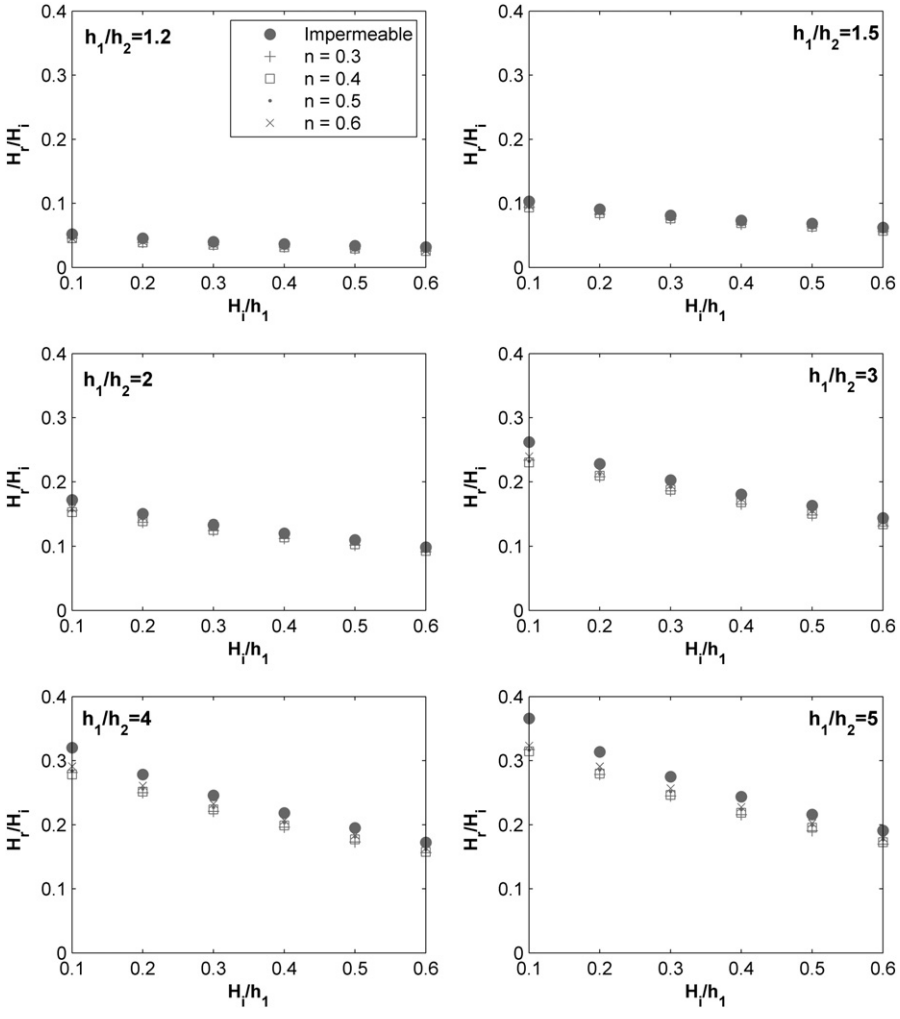

Fig. 11. Reflected solitary wave in front of the step for $D_{50}/h_1 = 0.2$. Several step characteristics (impermeable and porous) are plotted together.

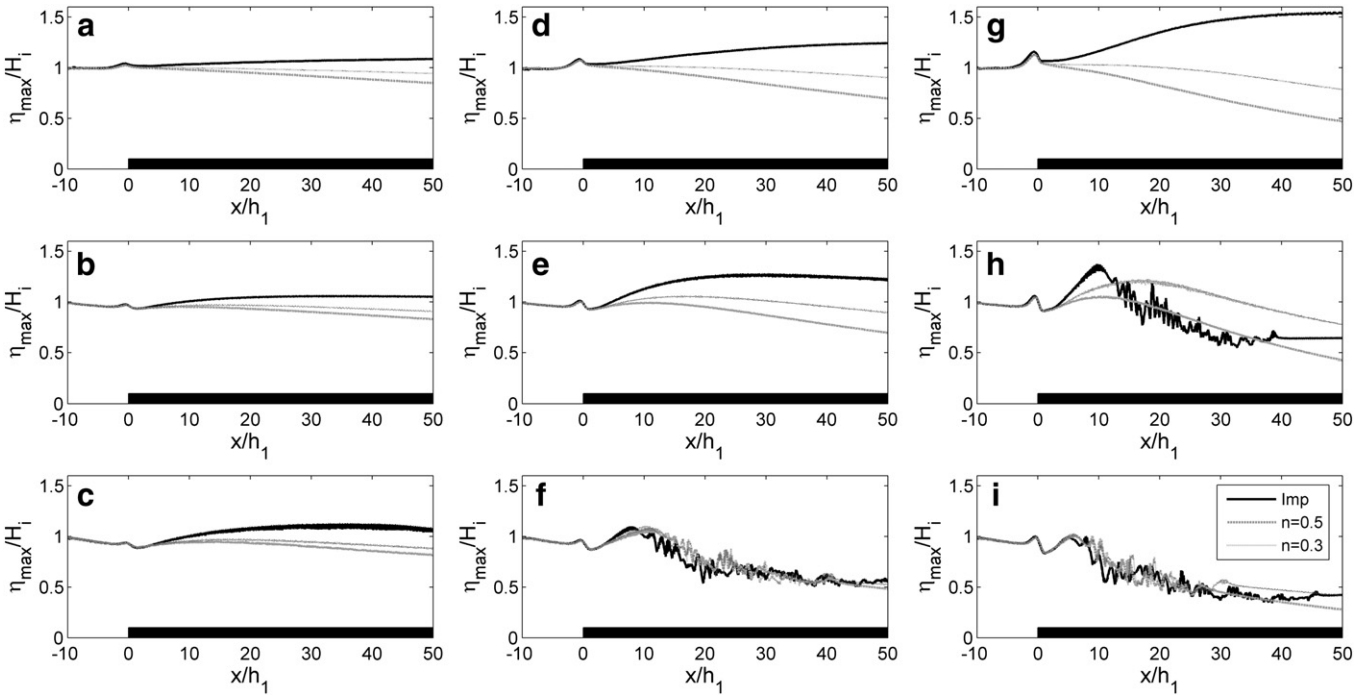

Fig. 12. Leading soliton evolution over impermeable (solid line) and permeable step. Dashed line: $n=0.5$ and $D_{50}/h_1=0.2$. Dotted line: $n=0.3$, $D_{50}/h_1=0.2$. (a) $h_1/h_2=1.2$, $H_i/h_1=0.1$; (b) $h_1/h_2=1.2$, $H_i/h_1=0.3$; (c) $h_1/h_2=1.2$, $H_i/h_1=0.5$; (d) $h_1/h_2=1.5$, $H_i/h_1=0.1$; (e) $h_1/h_2=1.5$, $H_i/h_1=0.3$; (f) $h_1/h_2=1.5$, $H_i/h_1=0.5$; (g) $h_1/h_2=2$, $H_i/h_1=0.1$; (h) $h_1/h_2=2$, $H_i/h_1=0.3$; and (i) $h_1/h_2=2$, $H_i/h_1=0.5$.

In this study we have investigated the effect of wave damping on solitary wave evolution and soliton disintegration over a porous step for both breaking and non-breaking solitary waves using Volume-Averaged Reynolds Averaged Navier–Stokes equations extending the focus of previous studies. Porous media induced damping is determined based on empirical formulations for relevant parameters showing a high degree of agreement with experimental results used for validation.

We have found that virtually in all cases, step height is the most relevant parameter to influence wave evolution. In the lower steps, damping affects wave height reduction during propagation, while a coherent fission into solitons is visible. In higher steps, wave behavior

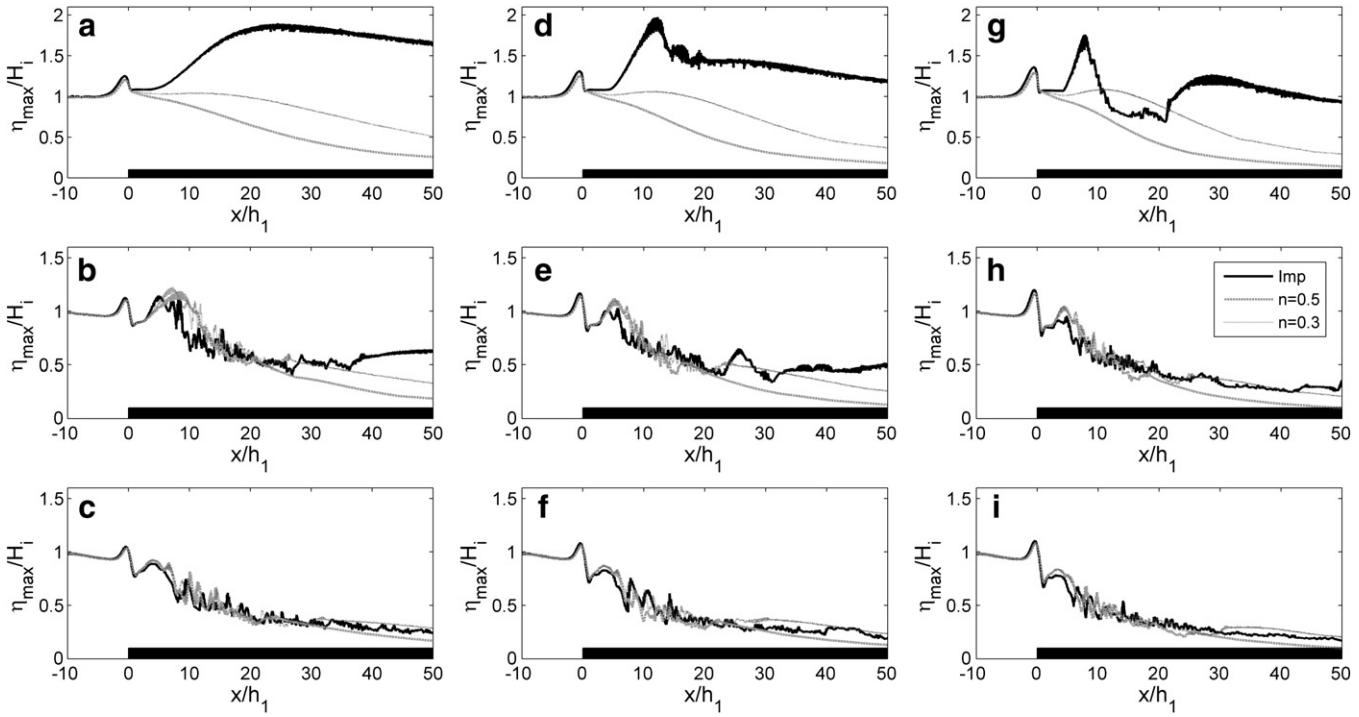

Fig. 13. Leading soliton evolution over impermeable (solid line) and permeable step. Dashed line: $n=0.5$ and $D_{50}/h_1=0.2$. Dotted line: $n=0.3$, $D_{50}/h_1=0.2$. (a) $h_1/h_2=3$, $H_i/h_1=0.1$; (b) $h_1/h_2=3$, $H_i/h_1=0.3$; (c) $h_1/h_2=3$, $H_i/h_1=0.5$; (d) $h_1/h_2=4$, $H_i/h_1=0.1$; (e) $h_1/h_2=4$, $H_i/h_1=0.3$; (f) $h_1/h_2=4$, $H_i/h_1=0.5$; (g) $h_1/h_2=5$, $H_i/h_1=0.1$; (h) $h_1/h_2=5$, $H_i/h_1=0.3$; and (i) $h_1/h_2=5$, $H_i/h_1=0.5$.

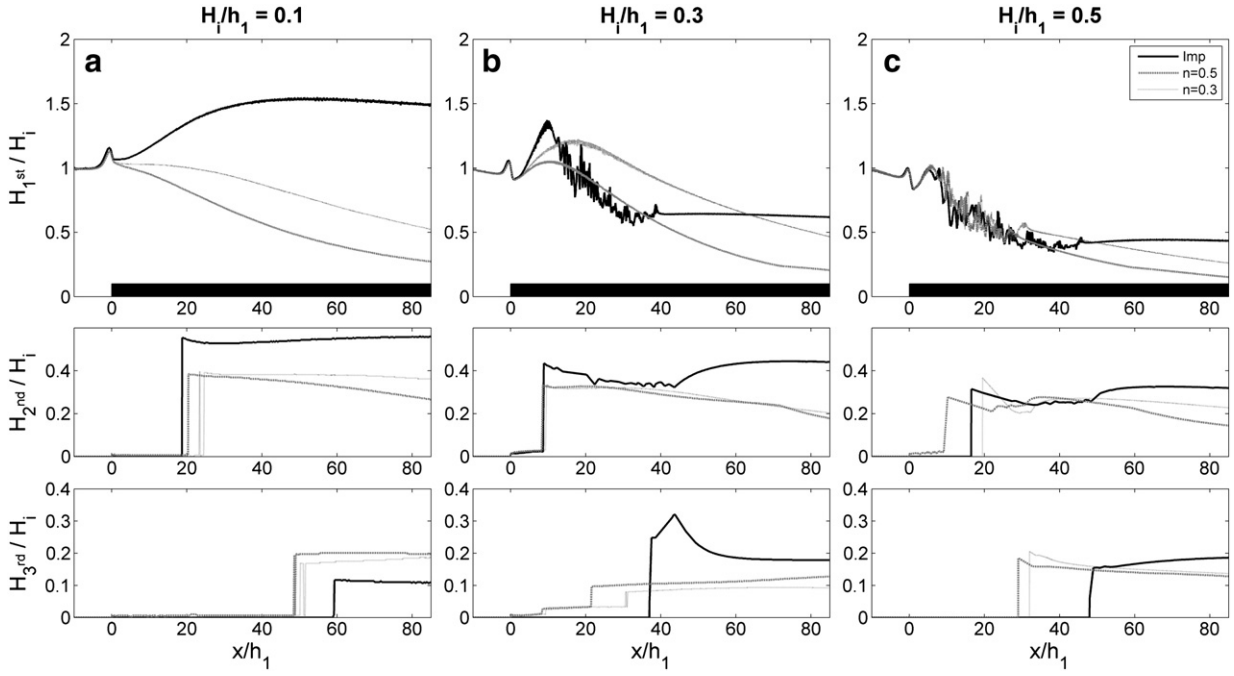

Fig. 14. Evolution of soliton amplitudes for a $h_1/h_2 = 2$ step: leading (upper panel), second (middle panel) and third (lower panel) for $H_i/h_1 = 0.1$ (left column), 0.3 (middle column) and 0.5 (right column). Solid line: impermeable step. Dashed line: $n = 0.5$ and $D_{50}/h_1 = 0.2$. Dotted line: $n = 0.3$, $D_{50}/h_1 = 0.2$.

is more significantly affected by damping, producing changes in the breaking type, from plunging to spilling, or also inhibiting breaking by the reduction of the wave peaking. Although fission is produced, a clear evolution of the individual solitons is not clearly visible due to the action of bed damping at higher steps.

Our results indicate that solitons propagate faster on a porous step when the non-linearity of the solitary wave is low. However, increasing nonlinearity results in faster soliton propagation over an impermeable step. In addition, it is found that increasing porosity and nominal diameter increases damping even in the presence of breaking, yielding consequently a reduction in solitons celerity.

The depth ratio h_2/h_1 appears to be the dominant parameter in the transmission and reflection coefficients even more than porosity or relative wave height H_i/h_1.

We have shown that the porous step also modifies the fission and the solitary wave disintegration process although the number of solitons is observed to be the same in both porous and impermeable steps. In the absence of breaking, porous bed triggers a faster fission of

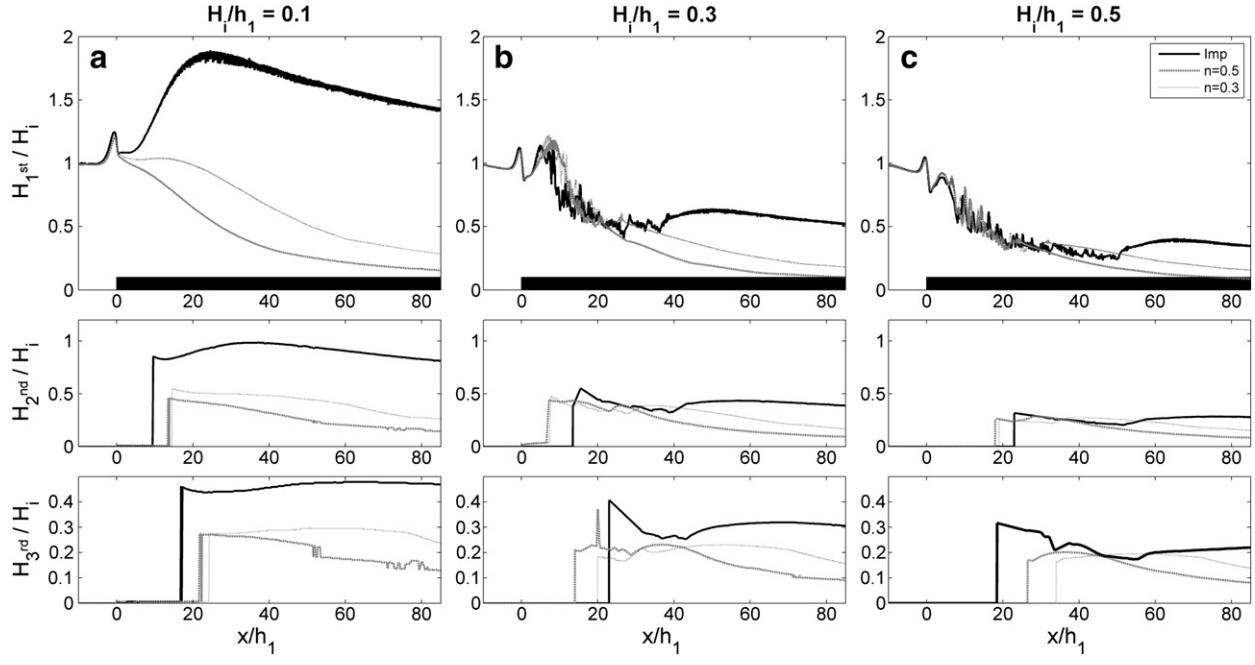

Fig. 15. Evolution of soliton amplitudes for a $h_1/h_2 = 3$ step: leading (upper panel), second (middle panel) and third (lower panel) for $H_i/h_1 = 0.1$ (left column), 0.3 (middle column) and 0.5 (right column). Solid line: impermeable step. Dashed line: $n = 0.5$ and $D_{50}/h_1 = 0.2$. Dotted line: $n = 0.3$, $D_{50}/h_1 = 0.2$.

the incident wave into a second and third solitons. When breaking appears, a more energetic breaking process can be identified on the impermeable bottom due to a lower bed friction and the lack of bed percolation. Furthermore, broken bore evolution is observed to be developed in a larger distance over impermeable steps.

As with regards solitons evolution along the step it is concluded that it is also affected by bed characteristics. Our numerical study indicates that, in the absence of breaking, the leading and the second solitons reduce their amplitude while propagating. This reduction is observed to increase with porosity. Moreover, the second soliton is released earlier on an impermeable step. When the wave height increases the role of the breaking process dominates over the wave dissipation on the porous bottom and slight differences are observed. Fission is produced earlier on a porous bed revealing a clear influence of the bottom characteristics on soliton generation. The amplitude of the second and third solitons is very similar in both impermeable and porous steps but they evolved differently due to the effect of bed damping.

In summary, it can be said that using VARANS equations is an excellent way to analyze the combined effect of solitary wave attenuation by porous damping and breaking.

Acknowledgments

J.L. Lara is indebted to the MEC (Ministerio de Educación y Ciencia, Spain) for the funding provided in the "Ramon y Cajal" Program (RYC-2007-00690). The work is funded by the projects BIA2008-05462 and CTM2008-06044 from the Ministerio de Ciencia e Innovacion (Spain).

References

Arbhabhirama, A., Dinoy, A.A., 1973. Friction factor and Reynolds number in porous media flow. ASCE J Hydraul Div. 99, 901–911.
Burcharth, H.F., Andersen, O.H., 1995. "On the one-dimensional steady and unsteady porous flow equations" Coastal Engineering, 24. Number 3, 233–257.
Chang, H.H., 2004, "Interaction of water waves and submerged permeable offshore structures" PhD Thesis, The National Cheng Kung University, Taiwan.
Corvaro, S., Mancinelli, A., Brocchini, M., Seta, E., Lorenzoni, C., 2010. On the wave damping due to a permeable seabed. Coastal Engineering 57, 1029–1041.
Goring, D., 1979, "Tsunamis—the propagation of long waves onto a shelf" PhD Thesis, California Institute of Technology, Pasadena, California.
Guanche, R., Losada, I.J., Lara, J.L., 2009. Numerical analysis of wave loads for coastal structure stability. Coastal Engineering 56 (5–6), 543–558.
Hsu, T.J., Sakakiyama, T., Liu, P.L.F., 2002. A numerical model for wave motions and turbulence flows in front of a composite breakwater. Coastal Engineering 46, 25–50.
Huang, C.J., Chang, H.H., Hwung, H.H., 2003. Structural permeability effects on the interaction of a solitary wave and a submerged breakwater. Coastal Engineering 49, 1–24.
Huang, C.J., Shen, M.L., Chang, H.H., 2008. Propagation of a solitary wave over rigid porous beds. Ocean Engineering. 35, 1194–1202.
Lara, J.L., Garcia, N., Losada, I.J., 2006a. RANS modelling applied to random wave interaction with submerged permeable structures. Coastal Engineering 53, 395–417.
Lara, J.L., Losada, I.J., Liu, P.L.F., 2006b. Breaking waves over a mild gravel slope: experimental and numerical analysis. Journal of Geophysical Research C: Oceans 111 Article number C11019.
Lara, J.L., Ruju, A., Losada, I.J., 2011. Reynolds averaged Navier–Stokes modelling of long waves induced by a transient wave group on a beach. Proceedings of the Royal Society A 467, 1215–1242.
Lee, J.J., Skjelbreia, J.E., Raichlen, F., 1982. "Measurement of velocities in solitary waves" Journal of the Waterway. Port, Coastal & Ocean Division 108, 200–218.
Lin, P., 2004. A numerical study of solitary wave interaction with rectangular obstacles. Coastal Engineering. 51, 35–51.
Liu, P.L.F., Cheng, Y., 2001. A numerical study of the evolution of a solitary wave over a shelf. Physics of Fluids 13, 1660–1667.
Losada, M.A., Vidal, C., Medina, R., 1989. Experimental study of the evolution of a solitary wave at an abrupt junction. Journal of Geophysical Research 94, 14557–14566.
Losada, I.J., Patterson, M.D., Losada, M.A., 1997. Harmonic generation past a submerged porous step. Coastal Engineering 31, 281–304.
Losada, I.J., Lara, J.L., Guanche, R., Gonzalez-Ondina, J.M., 2008. Numerical analysis of wave overtopping of rubble mound breakwaters. Coastal Engineering 55, 47–62.
McDougal, W.G., 1993. State of the art practice in coastal engineering. Lecture Notes, National Cheng Kung University, Taiwan, pp. 10.25–10.28.
Mei, C.C., 1985. Scattering of solitary wave at abrupt junction. J. Waterw. Port Coastal Ocean Engineering 3, 319–328.
Mei, C.C., Li, Y., 2004. "Evolution of solitons over a randomly rough seabed" Physical Review E. Statistical, Nonlinear, and Soft Matter Physics 70 016302.
Nakayama, A., Kuwahara, F., 1999. A macroscopic turbulence model for flow in a porous medium. Journal of Fluids Engineering 121, 427–433.
Pelinovsky, E., Choi, B.H., Talipova, T., Woo, S.B., Kim, D.C., 2009. Solitary wave transformation on the underwater step: asymptotic theory and numerical experiments. Applied Mathematics and Computation 217, 1704–1718.
Putnam, J.A., 1949. Loss of wave energy due to percolation in a permeable sea bottom. Trans. Am. Geophys. Union 30, 349–356.
Savage, R.P., 1953. "Laboratory study of energy losses by bottom friction and percolation" Beach Erosion Board. Corps of Engineers, Technical Memorandum. 31.
Sawaragi, T., Deguchi, I., 1992. "Waves on permeable layers" Proceedings 23rd Coastal Engineering Conference. ASCE, Venice. pp. 1531–1544.
Seabra-Santos, F.J., Renouard, D.P., Temperville, A.M., 1987. Numerical and experimental study of the transformation of a solitary wave over a shelf or isolated obstacles. Journal of Fluid Mechanics 176, 117–134.
Sollitt, C.K., Cross, R.H., 1972. Wave transmission through permeable breakwaters. Proc. 13th Coastal Engineering. Conf., (Vancouver) 3 July 10–14.
Torres-Freyermuth, A., Losada, I.J., Lara, J.L., 2007. Modeling of surf zone processes on a natural beach using Reynolds-Averaged Navier–Stokes equations. Journal of Geophysical Research C: Oceans 112 Article number C09014.
Torres-Freyermuth, A., Lara, J.L., Losada, I.J., 2010. Numerical modelling of short- and long-wave transformation on a barred beach. Coastal Engineering 57, 317–330.
van Gent, M.R.A.,1995, "Wave interaction with permeable coastal structures". Ph.D. Thesis, Delft University Press.
Whitham, G.B., 1974. Linear and nonlinear waves. SIAM Review 18, 776–781.